Biol Cybern (2012) 106:429–439
DOI 10.1007/s00422-012-0498-2

ORIGINAL PAPER

Biological Cybernetics

Inferior olive mirrors joint dynamics to implement an inverse controller

Rodrigo Alvarez-Icaza · Kwabena Boahen

Received: 11 January 2011 / Accepted: 30 May 2012 / Published online: 14 August 2012

Abstract To produce smooth and coordinated motion, our nervous systems need to generate precisely timed muscle activation patterns that, due to axonal conduction delay, must be generated in a predictive and feedforward manner. Kawato proposed that the cerebellum accomplishes this by acting as an inverse controller that modulates descending motor commands to predictively drive the spinal cord such that the musculoskeletal dynamics are canceled out. This and other cerebellar theories do not, however, account for the rich biophysical properties expressed by the olivocerebellar complex's various cell types, making these theories difficult to verify experimentally. Here we propose that a multizonal microcomplex's (MZMC) inferior olivary neurons use their subthreshold oscillations to mirror a musculoskeletal joint's underdamped dynamics, thereby achieving inverse control. We used control theory to map a joint's inverse model onto an MZMC's biophysics, and we used biophysical modeling to confirm that inferior olivary neurons can express the dynamics required to mirror biomechanical joints. We then combined both techniques to predict how experimentally injecting current into the inferior olive would affect overall motor output performance. We found that this experimental manipulation unmasked a joint's natural dynamics, as observed by motor output ringing at the joint's natural frequency, with amplitude proportional to the amount of current. These results support the proposal that the cerebellum—in particular an MZMC—is an inverse controller; the results also provide a biophysical implementation for this controller and allow one to make an experimentally testable prediction.

Rodrigo Alvarez-Icaza (✉) · Kwabena Boahen
Bioengineering Department, Stanford University, Stanford, CA, USA
e-mail: rodrigo.alvarez.i@gmail.com; boahen@stanford.edu
URL: http://www.stanford.edu/group/brainsinsilicon/

Keywords Motor cortex · Cerebellum · Spinal cord reflexes · Inverse control

1 Introduction

Whether we are trying to keep our gaze stable while moving our head or land a complex acrobatic maneuver on our feet, smooth and coordinated motion requires that our brains—the cerebellum in particular—issue precisely timed motor signals to our musculoskeletal system. Even ordinary everyday tasks such as reaching or walking become monumental motor control challenges when considering that dozens of muscle activations, across multiple joints, must be precisely sequenced and synchronized to achieve the desired trajectory or to produce the proper forces to balance and propel us forward. Muscles' slow response times [>25 ms (Bobet and Stein 1998)] and the long axonal conduction delays [∼10 ms for descending motor commands alone (Eyre et al. 1991)] required to drive them further complicate the problem, precluding fast control loops and thus favoring a predictive feedforward control strategy (Widrow and Walach 1996). To predict proper muscle activation sequences, the controller—in this case the cerebellum—must possess some knowledge of musculoskeletal dynamics' and to coordinate the motion, it must possess the means to precisely time its output. Learning to predict musculoskeletal dynamics to issue precisely timed motor commands is the role of the cerebellum, without which motion becomes erratic and imprecise (Ghez and Fahn 1985).

Existing cerebellar models fail to explain how the rich membrane dynamics observed in all neuron types within a cerebellar multizonal microcomplex (MZMC) (Apps and Garwicz 2005)—the loop formed by the deep cerebellar nucleus (DCN), inferior olive (IO), and Purkinje cells (PCs)—give rise to precisely timed motor signals. Inspired

by the anatomy, Marr (1969) and Albus (1971) considered neurons within the cerebellar network, PCs in particular, as instantaneous threshold elements that respond to the sensory context presented through parallel fibers. To produce motor sequences, their models require that motor commands change the sensory context, thereby triggering the next motor command, and so forth. Fujita (1982) proposed that Golgi cells delay sensory signals as they jump from mossy to parallel fibers, enabling PCs to learn spatiotemporal patterns. This idea inspired Barto et al. (1993) adjustable pattern generator model, which relies on network dynamics but still does not account for membrane dynamics. Kawato and Gomi mapped their feedback error-learning paradigm onto the cerebellar architecture (Kawato and Gomi 1992), claiming that motor errors encoded by climbing fibers train the cerebellar cortex to acquire a joint's inverse model. However, their mapping did not consider cellular dynamics. Only recently did Wetmore et al. (2008) and De Schutter and Steuber (2009) propose models where PC dynamics pause to unlock the DCN's membrane dynamics, allowing the latter to burst by rebounding from inhibition. Despite a developing trend toward more detailed biophysical properties, a biophysically based explanation of how an MZMC functions as a motor controller is still lacking.

In particular, cerebellar models downplay the ongoing effect of the IO's rich resonant membrane dynamics on motor signal timing and consider the IO as either relaying externally triggered training signals or generating an internal pacemaker clock. Subscribers to the Mars–Albus–Ito perspective entirely disregard the IO's membrane dynamics and simply consider the role of climbing fibers—all of which originate in the IO—as signaling motor performance errors (Simpson et al. 1996). Llinas' alternate view is that, through its extensive gap-junction network, the IO groups a set of muscles together to reduce the number of controllable degrees of freedom, and through its intrinsic subthreshold oscillations it clocks muscle activation at 10 Hz to discretize time into a small set of activation events (Llinas 2009; Welsh and Llinas 1997; Leznik et al. 2002; Llinas and Yarom 1986). Both of these views disregard the temporal interactions that occur between the IO's input and its ongoing membrane dynamics.

Here we propose that the IO's membrane dynamics, in particular its subthreshold oscillations, mirror a biomechanical joint's resonant dynamics, enabling an MZMC to implement the joint's inverse transfer function such that the cerebellum acts as an inverse controller. By modeling the biomechanics and inverting its transfer function, we arrive at an inverse controller whose architecture and dynamic properties map onto an MZMC's anatomy and physiology. This mapping supports the hypothesis that the IO mirrors the biomechanical joint's resonant dynamics and predicts how manipulating the biophysical properties that determine an IO cell's membrane dynamics—its oscillation frequency and damping ratio—will affect motor output. These results specifically predict that experimental manipulations that introduce a mismatch between an IO's frequency and a biomechanical plant's natural frequency will unmask a joint's dynamics such that the overall output will ring at the joint's natural frequency regardless of the IO's oscillation frequency.

2 Methods

2.1 Biomechanical modeling

We model a biomechanical joint as comprised of a spring, a damper, and a force-producing element acting on a mass; it is a simple model that suffices to reproduce its oscillatory nature. The dynamics of this simplified joint are thus described by $M\cdot\ddot{x}+\beta\cdot\dot{x}+K\cdot x=F(t)$, where K and β represent the muscles' elasticity and viscosity, respectively, M represents the mass, x is M's displacement, and $F(t)$ represents the net force produced by the antagonistic muscle pair acting around the joint (Fig. 1a, b). Through a Laplace transform, we obtain the transfer function $P(s)=X(s)/F(s)=\omega_n^2/(s^2+2\cdot\zeta\cdot\omega_n\cdot s+\omega_n^2)$, where the natural frequency is given by $\omega_n^2=K/M$ and the damping ratio by $\zeta=\beta/(2\cdot M\cdot\omega_n)$. In particular, we use an exemplary system comparable to an elbow joint (Lacquaniti et al. 1982; Bennett et al. 1992), modeled as a rotational analog of $P(s)$, where $I=0.072$ kg m^2, $\beta=0.483$ N m s/rad, and $K=26.266$ N m/rad represent the rotational equivalents of M, β, and K, respectively. These parameters yield $\omega_n=3$ Hz and $\zeta=0.17$. For this underdamped case ($0<\zeta<1$), the joint responds to a step change in force by undergoing a rapid displacement, overshooting its final value, and ringing at its natural damped frequency, before eventually settling down (Fig. 1e).

We model the spinal cord stretch reflex as a closed-loop proportional-derivative (PD) controller that improves the biomechanical joint's performance. The joint is now described by the transfer function

$$J(s)=\frac{X(s)}{C(s)}=\frac{(K_P+sK_D)P(s)e^{-t_{ff}s}}{1+(K_P+sK_D)P(s)e^{-(t_{ff}+t_{fb})s}},$$

where K_P and K_D are the controller's proportional and derivative gains, respectively, and t_{fb} and t_{ff} represent ascending and descending axonal-conduction delays, respectively (Fig. 1a, c). $J(s)$'s performance may be improved by increasing the loop's gains. However, conduction delays—unavoidable in biology—impose a limit beyond which the system would become unstable, manifested as ever-growing oscillations at the output. To have our exemplary system mimic the physiology, we choose $K_P=1$ N m/rad, so that the stretch reflex's implementation doubles the overall joint stiffness (Hoffer and Andreassen 1981; Bennett 1994; Allum and Mauritz 1984; Sinkjaer et al. 1988), and

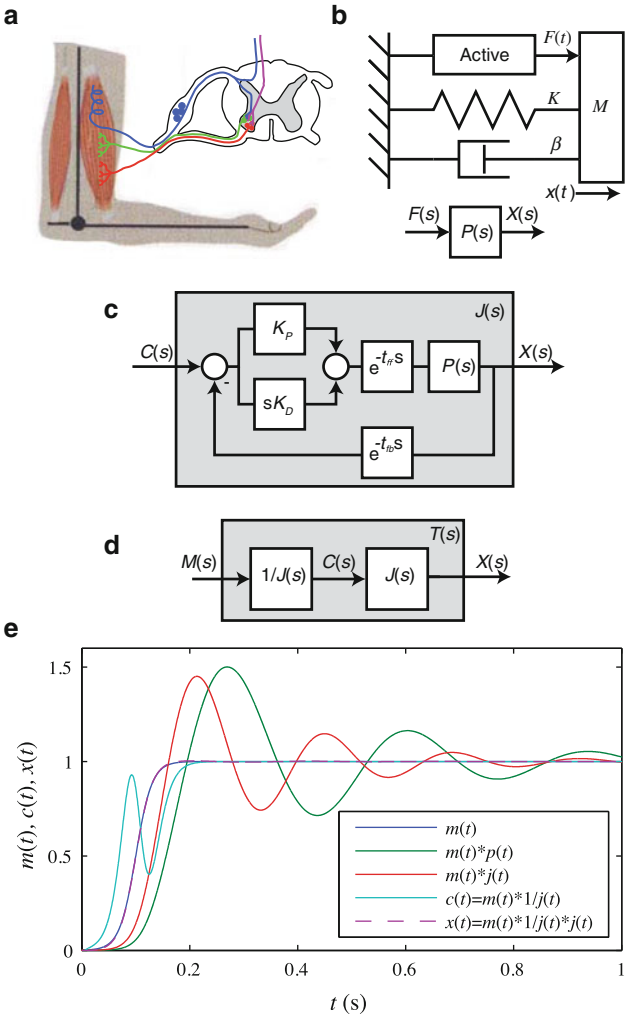

Fig. 1 Inverse control. **a** Spinal cord stretch reflex loop. **b** The joint's biomechanics $[P(s)]$ simplified as a spring with stiffness K, damper with damping coefficient β, and active force-producing element $[F(t)]$ arranged in parallel to drive a mass (M). **c** Stretch reflex modeled as a closed-loop controller with proportional and derivative gains K_P and K_D, and feedforward and feedback conduction delays t_{ff} and t_{fb}, around $P(s)$ $[J(s)]$. **d** Inverse control strategy where olivocerebellar complex intercepts descending motor commands, implementing $1/J(s)$. **e** Temporal response for $P(s)$, $J(s)$, $1/J(s)$, and $T(s)$ illustrating how $1/J(s)$ generates the optimal waveform $c(t)$ to predictively overdrive $J(s)$ so that its output $x(t)$ is a faithful copy of the overall system's input $m(t)$

$K_D = 0.0076$ N m s/rad, so that the overall joint's damping ratio remains at 0.17 (Lacquaniti et al. 1982; Weiss et al. 1988; Sinkjaer et al. 1988). Although this closed-loop controller does improve $P(s)$'s performance—by reducing overshoot and settling time so that the output trajectory matches more closely the desired motor command—it is constrained by instability, leaving room for further reduction of oscillations when compared with the full physiological response we wish to mimic.

To improve motor performance beyond the stability constraints faced by the closed-loop controller, we invert the joint's transfer function, literally by inverting $J(s)$. This inverse controller computes a signal that cloaks $J(s)$'s response by predicting its dynamics, making the overall system transparent from input to output. The controller's structure emerges directly from $1/J(s)$'s equation; it may be built from the same components found in $J(s)$ (Fig. 2a). Although we focus on the case with zero delay for simplicity, in general $1/J(s)$'s response $[C(s)$, (cyan trace in Fig. 1e)] predicts the proper input to $J(s)$ such that the overall output $[X(s)]$ perfectly matches the input $[M(s)]$.

Finally, we map the joint's inverse controller onto a cerebellar MZMC's architecture (Fig. 2). We do this by observing similarities between the inverse controller's structure and the MZMC's microcircuit: descending commands $[M(s)]$ arriving at the DCN are relayed to the IO and then looped back, through PCs at the cerebellar cortex, to the DCN. Along this loop, the IO mirrors $P(s)$'s oscillatory dynamics and PCs mirror spinal cord's loop gains, K_P and K_D. We propose that the MZMC's components—IO, PCs, and DCN—serve equivalent computational roles as blocks within the ideal inverse controller and, thus, together overcome the performance limitations of the spinal cord loop by computing $J(s)$'s inverse.

2.2 IO biophysical modeling

For parsimony, we chose the simplest possible IO model capable of generating oscillatory dynamics. Although more complex multicompartmental IO models that include spike generation via Na^+ and K^+ conductances are available (Schweighofer et al. 1999), these models have an immense parameter space that is a challenge to explore comprehensively. Manor's minimalistic model of IO cell subthreshold oscillations has only two conductances (Manor et al. 1997), and, remarkably, the theoretically predicted effects of modifying these conductances' strength (i.e., channel density) has been confirmed experimentally (Chorev et al. 2006).

We implement Manor (Manor et al. 1997) and Chorev's (Chorev et al. 2006) Hodgkin–Huxley-like IO model and analyze it as a 2D dynamical system. Their model, constructed by measuring T-type calcium channel dynamics in vitro (rat and guinea pig IO slices), describes an IO cell's membrane subthreshold dynamics as

$$
\begin{aligned}
&dV/dt = f(V,h) = 1/C_{\mathrm{m}} \\
&\quad \cdot \left[g_{\mathrm{T}} \cdot m \cdot h \cdot (V_{\mathrm{Ca}} - V) + g_{\mathrm{L}} \cdot (V_{\mathrm{L}} - V) + I_{\mathrm{app}} \right], \\
&dh/dt = g(V,h) = (h_\infty - h)/\tau_h, \\
&m = (1 + \exp\left[-(V + 55.6)/4.4204\right])^{-3}, \\
&h_\infty = (1 + \exp\left[(V + 71.3)/5.472\right])^{-1}, \\
&\tau_h = 30 + 30 \cdot \exp\left[(V + 160)/30\right] / \exp\left[(V + 89)/7.3\right]
\end{aligned}
$$

[reproduced from Chorev et al. (2006)], where V represents the membrane voltage; g_T, m, h, h_∞, τ_h, and $V_{\mathrm{Ca}} = 120$ mV respectively represent the T-channel's maximum conductance, its activation (considered instantaneous),

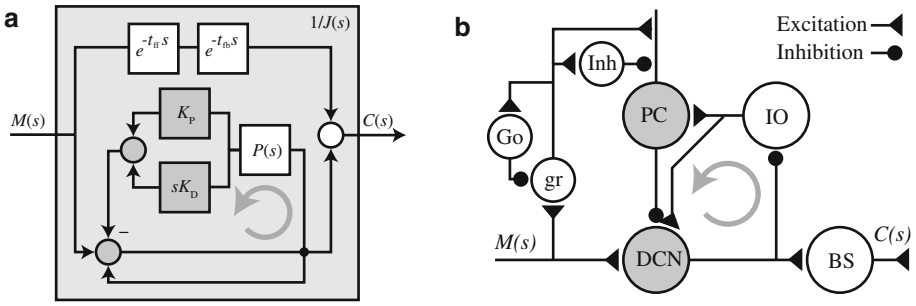

Fig. 2 A multizonal microcomplex maps to an inverse controller. **a** Block diagram for $1/J(s)$'s implementation illustrating a top path that mirrors $J(s)$'s total delay and a bottom path that mirrors the spinal cord's and the musculoskeletal dynamics. **b** Cerebellar MZMC diagram for comparison, illustrating an analogous loop around an MZMC that hypothetically computes $1/J(s)$. (DCN: deep cerebellar nucleus, BS: brainstem, IO: inferior olive, PC: Purkinje cells, Go: Golgi cells, gr: granule cells, Inh: inhibitory interneurons.

its inactivation, its steady-state inactivation, its inactivation time constant, and its reversal potential; g_L and $V_L = -60$ mV represent respectively the leak conductance and its reversal potential; I_{app} represents a generic input current (in μA/cm^2); and $C_m = 1\mu$F/cm^2 represents the membrane capacitance. Within these expressions, numerical parameters with dimensions of time or voltage are expressed in units of milliseconds or millivolts, respectively, and conductances in millisiemens/cm^2.

We linearize the model to determine the IO cell's natural frequency (ω_{IO}) and damping ratio (ζ_{IO}) for any given set of parameter values (g_T, g_L, and I_{app}). We first find the system's equilibrium points (V_{eq}, h_{eq}) by solving for the intersection between its V and h nullclines, using a properly seeded Newton–Raphson method. We then construct the system's linearized Jacobian at V_{eq}, h_{eq}

$$L(V_{eq}, h_{eq}) = \begin{bmatrix} \frac{\delta f}{\delta V}(V,h) & \frac{\delta g}{\delta V}(V,h) \\ \frac{\delta f}{\delta h}(V,h) & \frac{\delta g}{\delta h}(V,h) \end{bmatrix}$$

and call Matlab's built-in function eig(L) to calculate its eigenvalues (λ_1, λ_2). These eigenvalues describe the model's response as $V(t) = c_1 \cdot \exp(\lambda_1 \cdot t) + c_2 \cdot \exp(\lambda_2 \cdot t)$ (Izhikevich 2007) and give its natural frequency and damping ratio: $\omega_{IO} = (\lambda_1 \cdot \lambda_2)^{-1/2}$ and $\zeta_{IO} = -(\lambda_1 + \lambda_2)/(2 \cdot \omega_{IO})$, expressions that are valid for all possible eigenvalues. Unlike the typical approach of characterizing IO oscillatory dynamics by their decay time constant (determined by $\lambda_{1,2}$'s real component) and their natural damped frequency (determined from $\lambda_{1,2}$'s imaginary component), characterizing IO subthreshold dynamics with ω_{IO} and ζ_{IO} allows for a direct comparison with $P(s)$'s fundamental parameters (ω_n and ζ).

To determine the full range of values an IO expresses for ω_{IO} and ζ_{IO}, we explore the model's parameter space, varying g_T, g_L, and I_{app} over physiologically plausible ranges (Chorev et al. 2006). We first sweep g_T and g_L without injecting current and classify the responses as overdamped ($\zeta_{IO} > 1$), underdamped ($0 < \zeta_{IO} < 1$), or undamped ($\zeta_{IO} < 0$) (Fig. 3a1, a2). Within each region, we choose exemplary points (g_T, g_L pairs), simulate the transient response for various I_{app} values (Fig. 3b1, b2), and compute I_{app}'s effect on ω_{IO} and λ_{IO} (Fig. 3c1, c2). Finally, we explore the IO's full range by simulating the effect of a maximum and minimum applied current ($I_{app} = \pm$ 1μ A/cm^2) for all g_T, g_L pairs (Fig. 4).

2.3 Mirroring joint dynamics

To compare an IO's expressible ω_{IO} and ζ_{IO} range to a joint's physiological ω_n and ζ range, we represent them graphically (Fig. 4). To do this, we plot all ω_{IO} versus ζ_{IO} pairs found for the entire g_T, g_L simulation range and manually trace a contour over all the samples from the simulation results to define three regions: one region for samples where $I_{app} = 0$, one for $I_{app} = 1\ \mu A/\text{cm}^2$, and one for $I_{app} = -1\ \mu A/\text{cm}^2$. For comparison, we plot experimentally measured ω_n and ζ for the physiological human ankle (Gottlieb and Agarwal 1978; Weiss et al. 1988; Hunter and Kearney 1982; Aruin and Zatsiorsky 1984; Allum and Mauritz 1984; Sinkjaer et al. 1988), knee (Zhang et al. 1998), elbow (Lacquaniti et al. 1982; Bennett et al. 1992), wrist (Sinkjaer and Hayashi 1989), and finger (Becker and Mote 1990) joints, and we manually trace an estimated region around each joint's data samples.

2.4 Mismatch's effect on overall motor output

To characterize the effect of an imperfect inverse transfer function implementation on overall motor performance, we introduce a mismatch between ω_{IO} and ω_n or between ζ_{IO} and ζ. Using Matlab's Control System Toolbox, we implement $T(s) = [1/J'(s)] \cdot J(s)$ for various amounts of mismatch and simulate $T(s)$'s transient and frequency response using Matlab's built-in functions, sim() and bode(), respectively. As a step input demands infinite torque, we instead use a sigmoid, described by $m(t) = 1/(1 + \exp(-(t - t_0)/\tau))$, and choose

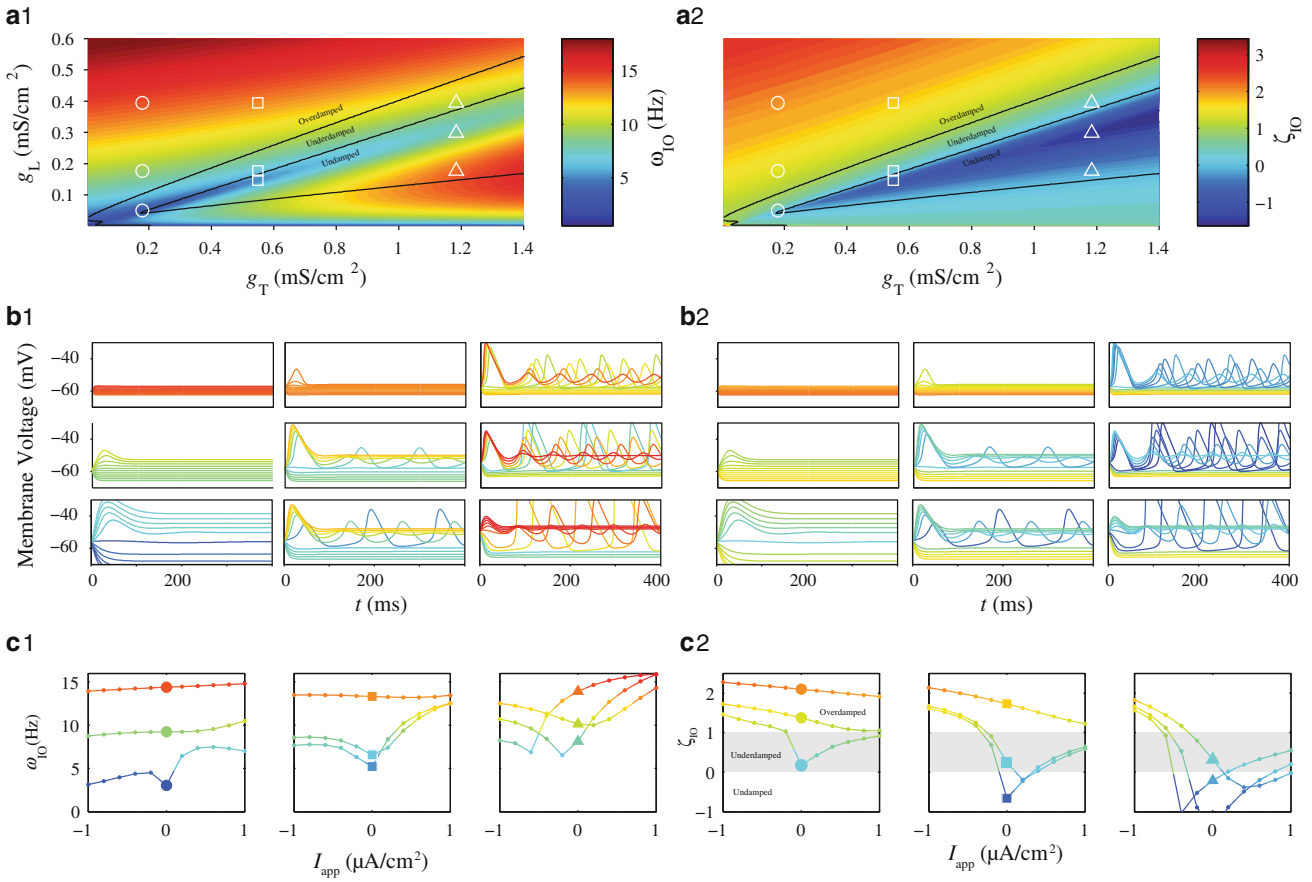

Fig. 3 Inferior Olive (IO) dynamics. **a1** Natural oscillation frequency (ω_{IO}) and **a2** damping ratio (ζ_{IO}) for IO neurons with various combinations of leak (g_L) and calcium (g_T) conductances (zero applied current), computed from eigenvalues at the system's equilibrium point. **b1** and **b2** Transient responses to current injections ($I_{\text{app}} = -1$ to 1 μA) for points highlighted in **a1** and **a2**; *color* represents, ω_{IO} and ζ_{IO}, respectively, and subpanel locations correspond marker locations in **a1** and **a2**. **c1** ω_{IO} and **c2** ζ_{IO} as a function of I_{app} for the same points.

$\tau = 15$ ms such that the torque from the exemplary elbow joint never exceeds 40 N m (t_0 simply delays the input's onset by 100 ms). Using the waveforms obtained from transient simulations, we measure the motor output's maximum percentage overshoot, rise time (from 10 to 90 %), and settling time (to within a $\pm$ 5 % error band) as a function of mismatch between ω_{IO} and ω_n or between ζ_{IO} and ζ.

We model the effect of experimental current injection into IO on motor performance, $T(s)$, by determining how it changes $J(s)$. We begin by choosing an IO cell configuration that exactly mirrors the exemplary joint's dynamics ($P(s)$). In particular, $g_{\text{T}} = 0.1792$ and $g_{\text{L}} = 0.05$ mS/cm^2 yields $\omega_{\text{IO}} = \omega_n = 3.04$ Hz and $\zeta_{\text{IO}} = \zeta = 0.1756$ (bottom left circle in Fig. 1a1, a2). For this specific configuration, we sweep I_{app} over a $\pm 0.2 \mu A/cm^2$ range, compute ω_{IO} and ω_{IO}, adjust $J(s)$ accordingly, and then compute $T(s)$'s temporal and frequency responses. The temporal responses predict performance (maximum percentage overshoot, rise time, and settling time) as a function of I_{app}.

3 Results

One strategy to overcome the performance limitations of the spinal cord's closed-loop controller is to drive it through its inverse transfer function, which we found maps to a cerebellar MZMC. The inverse transfer function $[1/J(s)]$ emerges naturally from inverting the spinal cord's closed-loop transfer function $[J(s)]$, and therefore consists of the same components now arranged along two distinct pathways. One pathway matches the spinal cord's total delay, whereas the other pathway forms a loop that inverts the joint's dynamics. This loop is remarkably similar to the loop that defines an MZMC's architecture (Fig. 1). Around these similar loops, the IO mirrors the biomechanical joint's oscillatory dynamics $[P(s)]$, PCs mirror the spinal cord's loop gains (K_{P} and K_{D}), and the DCN integrates descending input and feedback from the IO to produce the final output that projects to the brainstem (Fig. 2). By mirroring $J(s)$'s dynamics, $1/J(s)$ (or an MZMC) overdrives $J(s)$, cloaking its natural response such

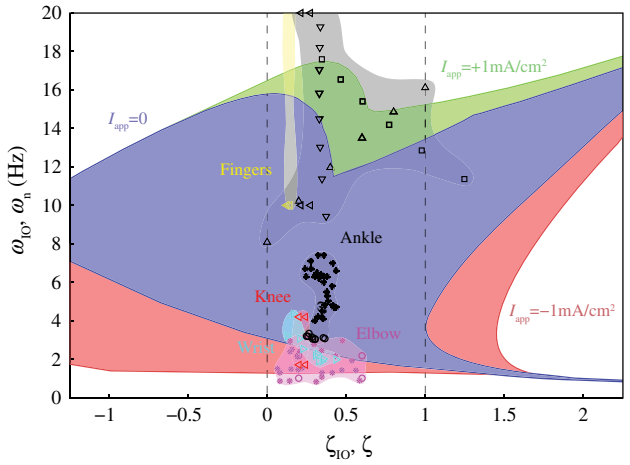

Fig. 4 Mirroring joint dynamics. Contour plot illustrating ω_{IO} and ζ_{IO} combinations achievable by rat IO neurons in comparison with human natural frequency (ω_n) and damping ratio (ζ) for ankle Gottlieb and Agarwal 1978; Aruin and Zatsiorsky 1984; Allum and Mauritz 1984; Sinkjaer et al. 1988; Weiss et al. 1988, knee Zhang et al. 1998), elbow Lacquaniti et al. 1982; Bennett et al. 1992, wrist (Sinkjaer and Hayashi 1989), and fingers (Becker and Mote 1990). Applying positive (+1 mA/cm^2, *green*) or negative (−1mA/cm^2, *red*) current expands the IO's range

that the overall system becomes transparent and thus outputs a faithful copy of the input (Fig. 1).

Although our mapping assigns specific roles to each cell type within an MZMC, here we focus on the IO as it is the most salient link between the inverse transfer function $[1/J(s)]$ and an MZMC's biophysics—specifically, both the IO and a biomechanical joint $[P(s)]$ are damped oscillators. In particular, the IO's unique oscillatory dynamics stand out as a direct match to the musculoskeletal system's oscillatory dynamics. Our mapping's prediction that, for an MZMC to implement a joint's inverse transfer function, the DCN implements proportional and derivative gains is explored in a companion paper (Alvarez-Icaza and Boahen 2011).

Mapping a joint's inverse transfer function to an MZMC requires that the IO's subthreshold dynamics match the biomechanical joint's natural frequency (ω_n) and damping ratio (ζ). In humans, for small perturbations, joints such as the ankle, wrist, elbow, and fingers are well described by a second-order system (Gottlieb and Agarwal 1978; Hunter and Kearney 1982; Lacquaniti et al. 1982; Allum and Mauritz 1984; Aruin and Zatsiorsky 1984; Weiss et al. 1988; Sinkjaer and Hayashi 1989; Becker and Mote 1990). Depending on the joint, ω_n may be between 1 and 30 Hz and ζ between 0.06 and 0.4; these values also depend on the joint's angle, displacement amplitude, and voluntary stiffening (Lacquaniti et al. 1982).

A biophysical IO model suggests that matching can be achieved by varying the amount of leak (g_L) and calcium (g_T) conductances expressed as well as the tonic input current (I_{app}). This simple model ignores Na^+ spikes and gap-junction coupling. Ignoring Na^+ spikes is justified if they serve purely as a readout mechanism—a phenomenon observed in vivo where axonal bursts ride atop subthreshold oscillation to encode phase or amplitude but do not disrupt the underlying period (Mathy et al. 2009). Ignoring gap-junction coupling is justified if the population's behavior is captured by a single IO cell with average properties—; Manor et al. 1997 showed that this is indeed the case.

We studied the biophysical IO model's response as g_T and g_L varied over the physiologically plausible ranges, focusing on underdamped subthreshold oscillations ($0 < \zeta_{IO} < 1$). We found that underdamped oscillations occurred with ω_{IO} ranging from 2 to 15 Hz. Furthermore, we found that $I_{app}(-1\text{to}1\,\mu A/cm^2)$ could alter ω_{IO} by up to a factor of 2 (and ζ_{IO} by 5), resulting in a total ω_{IO} range of 1 to 17 Hz for underdamped oscillations. Overall, assuming similar IO physiology in rats and humans (Sect. 4), these results suggest that IO cells ω_{IO} and ζ_{IO} can match the spectrum of biomechanical ω_n and ζ, as predicted by our mapping (Figs. 3, and 4).

Our MZMC model predicts that a mismatch between ω_{IO} and ω_n or between ζ_{IO} and ζ will unmask $J(s)$'s natural response, as seen by overall output ringing at ω_n, with amplitude proportional to the mismatch. We deliberately implemented an imperfect inverse transfer function—one in which the IO's parameters (ω_{IO} and ζ_{IO}) did not match the biomechanics fundamental parameters (ω_n and ζ)—and characterized the effect of mismatch on overall motor output. Mismatch, either between natural frequencies or damping ratios, introduces output ringing, always at a joint's natural frequency. This is easily observed for all mismatch cases, in transient analysis, where the waveform's peaks and troughs line up—albeit phase shifted—with $J(s)$'s natural response (Fig. 5); the amplitude is proportional to the amount of mismatch. A natural frequency mismatch has a much stronger effect on percentage overshoot than a damping ratio mismatch. Other output characteristics are also affected by mismatch: the output's settling time is weakly affected by a damping ratio mismatch, but it grows longer (showing abrupt steps when an oscillation's peak crosses beyond the ±5 % error band) with an increasing natural frequency mismatch, and the output's rise time grows for ω_{IO} faster than for ω_n but decreases for ζ_{IO} larger than for ζ. Altogether, the strongest effect is that of a natural frequency mismatch on motor output percentage overshoot (Fig. 5).

Our MZMC model's predictions can be tested experimentally by injecting current into an IO to perturb ω_{IO} and ζ_{IO}. To evaluate the effects that experimentally injecting current—by electrical stimulation or optogenetic techniques—into a population of IO cells would have on motor output performance, we implemented an inverse transfer function where ω_{IO} and ζ_{IO} were functions of current injection (I_{app}), as determined using Manor and Chorev's IO model. Simulating I_{app}'s effects on the IO (Fig. 3c), and then substituting

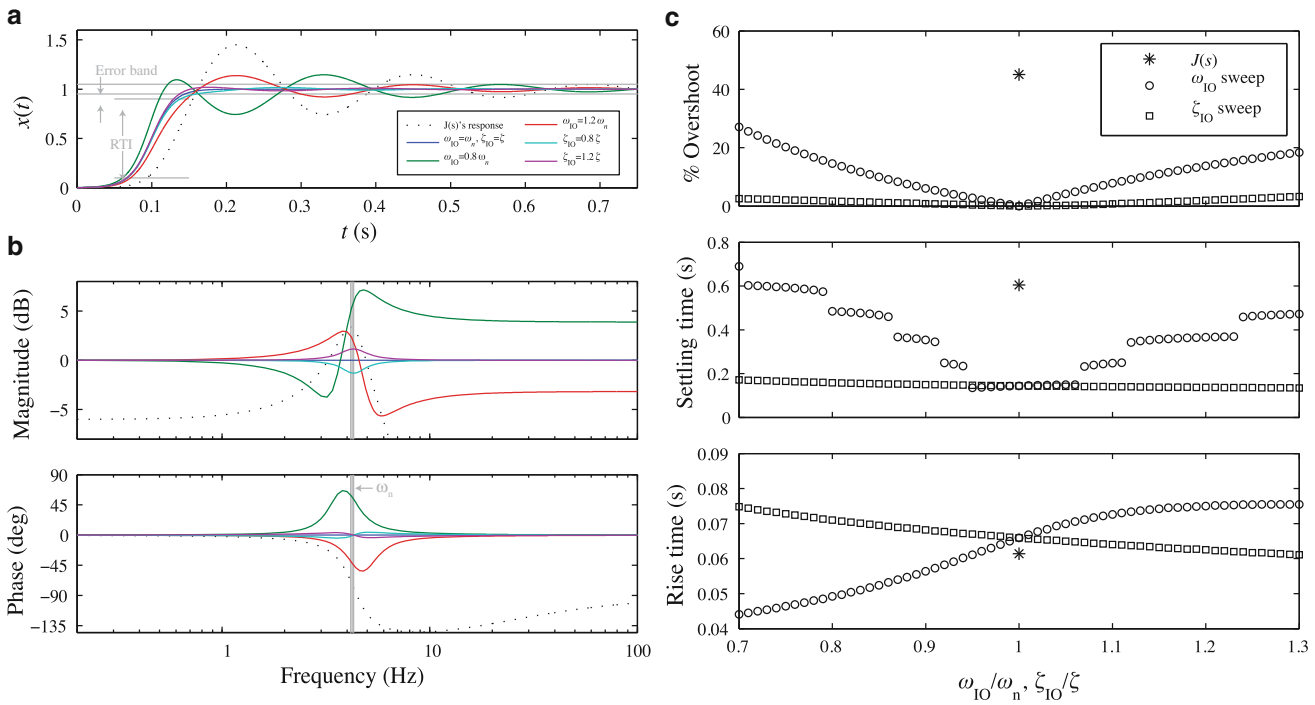

Fig. 5 Unmasking the joint dynamics. **a** $T(s)$'s temporal response to a smoothed input step where there is a simulated mismatch between an IO's oscillation frequency (ω_{IO}) and the biomechanical natural frequency (ω_n), or between the IO's damping ratio (ζ_{IO}) and the biomechanical damping ratio (ζ). *RTI*: range over which rise time is computed. **b** $T(s)$'s frequency response for same cases as in **a**, illustrating how mismatch unmasks a joint's natural response. **c** Output percentage overshoot, settling time, and rise time as a function of mismatch between oscillation frequencies or between damping ratios. The steplike behavior observed in the settling time is due to the peaks of later cycles of the oscillatory waveform abruptly crossing to the outside of the error band as the overall amplitude of the oscillation's overshoot grows

the resulting ω_{IO} and ζ_{IO} into $1/J(s)$, predicts that I_{app} will introduce motor output ringing at ω_n, with the amplitude rising with I_{app}'s magnitude, but quickly saturating (Fig. 6). Similarly, the settling time increases with I_{app}'s magnitude, whereas a positive current increases the rise time and a negative current decreases it. These effects saturate for currents larger than 0.15 A/cm^2. Using the results from the IO biophysical model to define $1/J(s)$, we establish a direct link between I_{app} and its associated effects on overall motor output and make experimentally testable predictions.

4 Discussion

While previous analyses focused on the IO's ability to sustain subthreshold oscillations, we studied the IO's ability to express the damped (nonsustained) oscillations appropriate for mirroring a joint's dynamics. Initially, inspired by the anatomy, the IO was considered to be a source of training signals to the cerebellar cortex (Marr 1969; Albus 1971); however, this view changed drastically when physiological recordings revealed the IO's unique ability to sustain subthreshold oscillations (Llinas and Yarom 1986). Despite the fact that only 15 % of IO slices have neuron pools that sustain spontaneous oscillations (Devor and Yarom 2002), sustained oscillations quickly became the focus of attention, repositioning IO as a timekeeper at the expense of disregarding its full dynamical repertoire. In particular, through biophysical modeling, Manor explains how gap junctions among a heterogeneous network of IO cells are required to generate sustained oscillations at the network level, and Chorev explains how the leak and T-channel conductances may be modulated to sustain oscillations. Manor and Chorev both disregard the IO's ability to act as a damped oscillator. We rectified that oversight by using their computational model to analyze the regime in which the IO acts as a damped oscillator, suitable for mirroring biomechanical dynamics.

We presented results showing that manipulating the IO's oscillation frequency and damping ratio—either by manipulating its conductances or by injecting current—results in motor output ringing at a joint's natural frequency. Analytically, regardless of the source of mismatch, $T(s)$'s output always rings at a joint's natural frequency because $J(s)$'s poles determine the system's overall poles; therefore, when $J(s)$'s poles are not perfectly canceled, they cause the system to ring at ω_n. For the case where $\zeta_{IO} < \zeta$, the gain at ω_n is less than one; hence we see a notch in the frequency response instead of a resonance (i.e., a peak). This is because the sys-

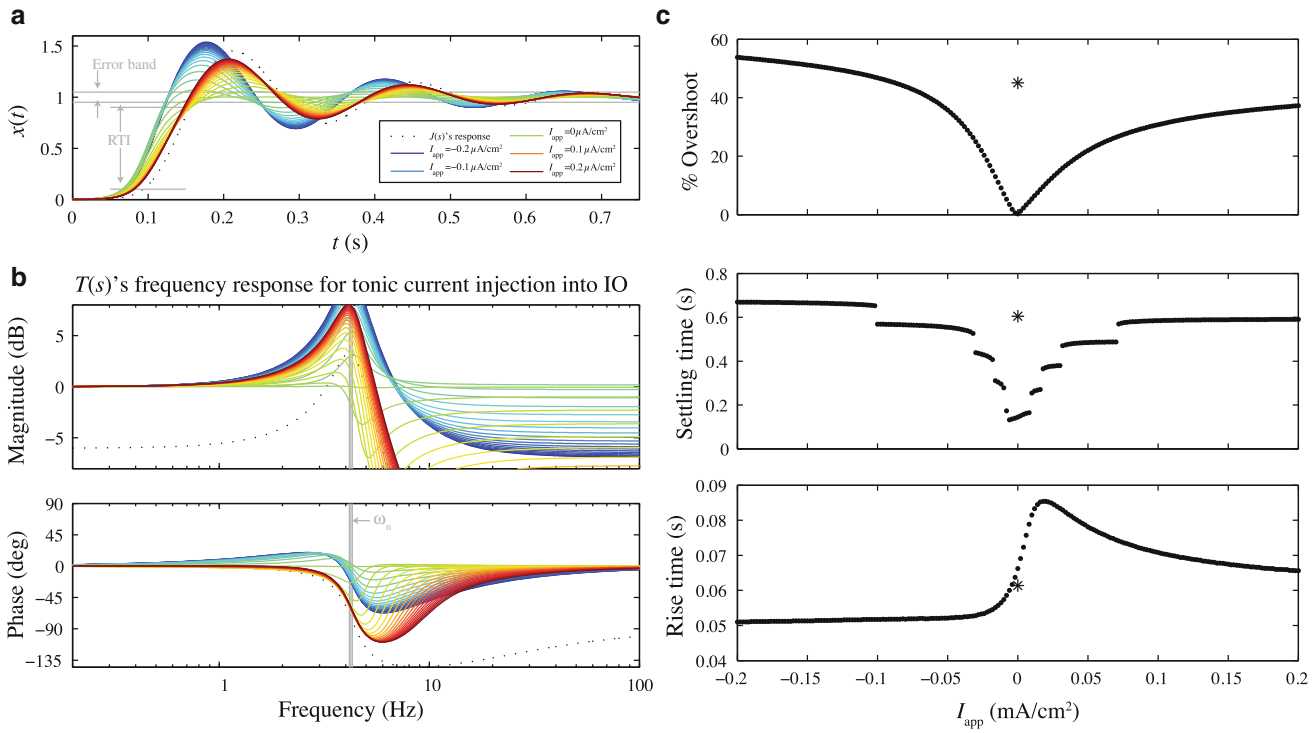

Fig. 6 Disturbing IO, experimental predictions **a** $T(s)$'s temporal response to a smoothed input step when tonic current is injected (I_{app}) to induce mismatch between IO's dynamics and the biomechanic's dynamics. *RTI* range over which rise time is computed. **b** $T(s)$'s frequency response for same cases as in (**a**), illustrating the unmasking of the joint's natural response. (**c**) Output's percent overshoot, settling time and rise time as a function of I_{app}. The step-like behavior observed in the settling time is due to the peaks of later cycles of the oscillatory waveform abruptly crossing to the outside of the error band as the overall amplitude of the oscillation's overshoot grows.

tem's overall gain is dominated by the ratio of dampening ratios, in particular $T(j\omega_n) = (\zeta_{\text{IO}} - G)/(\zeta - G)$, where $G = jK_P - K_D\omega_n$. However, in the time domain there is still ringing at ω_n because this notch subtracts ω_n from the step response, which is then described by $\underline{m}(t)$–$\sin(\omega_n t)$ (Fig. 5). Overall, conductance manipulation varies ω_{IO} and ζ_{IO} over the observed range of ω_n and ζ. Current injection also varies ω_{IO} and ζ_{IO} but has a much stronger effect on ζ_{IO} (Fig. 3). Remarkably, regardless of which parameter is mismatched, or the amount of current injected, motor output always rings with a frequency of ω_n (Fig. 6).

Our model predicts that, across species, the IO must match a joint's dynamics, yet we presented results comparing rat IO dynamics to human joint dynamics. As much as we would have liked to compare rodents to rodents and primates to primates, there is currently no literature describing subthreshold IO behavior in primates or joint dynamics in rodents. Our rodent–primate comparison is justified if two assumptions hold. First, IO cells' biophysics are conserved across mammals, and therefore IO dynamics are similar for all species regardless of size. Second, joint dynamics fall within this conserved IO frequency range regardless of animal size. Support for the first assumption will remain pending the unlikely availability of IO slice recordings from larger animals. Support for the second assumption comes from the fact that, although somewhat counterintuitively, the frequencies at which even the smallest mammals move rarely go beyond 10 Hz; mice in particular may run with stride frequencies of up to 11 Hz (Herbin et al. 2004), but their typical gait is approximately 5 Hz (Amende et al. 2005). Furthermore, legged-locomotion studies show that, in animals ranging from cockroaches to kangaroos, leg stiffness is proportional to body mass, rendering natural frequencies relatively constant (Blickhan and Full 1993).

Unlike IO subthreshold oscillations serving simply as a clock, our results argue that they actually serve to reproduce a limb's resonant dynamics. In the clock hypothesis, first proposed by Welsh and Llinas, muscle activation strengths are read out from the cerebellar cortex at discrete time intervals, clocked by IO spikes (Llinas and Welsh 1993; Welsh et al. 1995; Welsh and Llinas 1997). This model can produce arbitrary muscle activation patterns at the cost of requiring extensive storage within the cerebellar cortex. In our hypothesis, the IO solves the differential equations that describe

a joint's biomechanics, functioning as an analog computer, and the cerebellar cortex modulates IO output to implement the gains of the spinal cord stretch reflex. Our model better utilizes (and accounts for) the IO's rich temporal dynamics, at the cost of limiting the available waveforms.

Despite the longstanding belief that the IO only provides error signals to train the cerebellar cortex, predictions that the IO internally mirrors a joint's dynamics are also consistent with physiological evidence. Following Albus' proposal (Albus 1971), the IO has been considered the source of error signals to train the cerebellar cortex—a perspective supported by evidence that climbing fibers weaken parallel-fiber synapses onto PCs (Ito and Kano 1982) and that PC complex spiking increases during motor learning tasks (Gilbert and Thach 1977; Ojakangas and Ebner 1992). Nevertheless, consistent with the model's predictions, physiological recordings from PCs in monkeys during reaching tasks clearly show an increase in complex spiking prior to or during the earliest phase of motor initiation, with such increase being most significant for rapid or ballistic motions (Mano et al. 1986) where joint dynamics play a greater role in motion execution. In particular, detailed analysis of complex spiking during reaching tasks has revealed that, during the earliest phase of motion initiation, complex spikes encode the target's absolute position and that upon completing the reach, complex spikes encode the relative error to the target (Kitazawa et al. 1998).

Our results raise the question of how the IO transmits the phase and amplitude of its subthreshold oscillations, with frequencies above 3 Hz, to the cerebellum, using spikes that on average occur at <2 Hz (Gilbert and Thach 1977; Mano et al. 1986; Ojakangas and Ebner 1992; Kitazawa et al. 1998). The population of approximately 100 IO cells (Llinas et al. 2004) that belong to an MZMC can achieve this through their spike rate or spike timing. In rate coding, the number of spikes that occur across a population encodes the subthreshold oscillations' amplitude from instant to instant—, that is, the subthreshold waveform. This is possible because the cells' spikes occur independently, even though their subthreshold oscillations are tightly synchronized via gap junctions (Llinas and Yarom 1986; Leznik et al. 2002; Devor and Yarom 2002; Yarom and Cohen 2002). For instance, a different subset of ten cells would fire on each cycle, and their ten spikes would be distributed in time so as to reflect the oscillation's instantaneous amplitude throughout that cycle. Together, these ten subsets represent a 10 Hz subthreshold oscillation's amplitude and phase whereas individual cells only fire at 1 Hz. As an oscillation dampens, fewer cells fire in each subset, encoding its decreasing amplitude. In timing coding, the cells would always spike at a particular phase of the oscillation (Jacobson et al. 2009) but produce a burst of spikes, with the number of spikes increasing with the oscillation's amplitude (Mathy et al. 2009). Specifically, in vivo, a single somatic spike becomes an axonal burst, and this code is reliably transmitted to PCs, as observed in the duration of the resulting complex spike.

Our MZMC model predicts that for smooth motion to ensue, an MZMC's inverse transfer function must match a joint's dynamics. External changes, such as picking up an object, or internal changes, such as flexing the elbow, continuously change the joint's dynamics—in particular $P(s)$'s ω_n and ζ. The most direct strategy for the cerebellum to compensate for these ever-changing dynamics would be to mirror the changes by adapting the IO's ω_{IO} and ζ_{IO}. This could be achieved by varying the amount of tonic input into the IO, and thus the average applied current (I_{app}), to instantaneously change the dynamics of the cell (Fig. 4) to track the joint's ω_n and ζ. Alternatively, to track a joint's dynamics, the cerebellum may altogether recruit a different MZMC—also associated to the joint in question—tuned to the proper dynamics. As indeed we are capable of producing smooth motion under widely diverse external and internal dynamic configurations, to match these ever-changing joint dynamics, the cerebellum must somehow select or modulate the proper MZMC.

Our MZMC model may be tested by experimentally manipulating a joint's dynamics. Even though our MZMC model does not incorporate the role of ascending feedback from the spinal cord, it can account for the final state reached through adaptation. This adaptation may occur in the same MZMC that served that joint previously or it may occur in a different MZMC, depending on the cerebellum's adaptation strategy. Therefore, our model will predict that either the MZMC will change to match the new joint's dynamics or it will go silent. If an MZMC's activity did not adapt or go silent, this would invalidate our model.

Overall, our mapping between an MZMC and an inverse transfer function provides a mechanistic explanation that supports the hypothesis of the cerebellum as an inverse controller. Unlike most associative cerebellar models that imply the learning of stereotypical temporal patterns, our model suggests that an MZMC—through its dynamics—acts as an analog computer that implements a joint's inverse transfer function in real time. Our proposed implementation goes beyond abstract cerebellar models in that, at a mechanistic level, it is inspired by, and accounts for, membrane dynamics within the olivocerebellar loop, where in particular we have focused on the similarities between a joint's dynamics and the IO's dynamics. Inevitably, the cerebellum must generate appropriate temporal patterns to drive the joints; however, unlike other such models where patterns are stored as a sequence of activations, at a mechanistic level we propose that these patterns are computed in real time by the intrinsic dynamics within the system. Overall, the results so far suggest that biophysically mirroring a joint's dynamics internally may implement an inverse controller efficiently.

References

Albus J (1971) Theory of cerebellar function. Math Biosci 10(1/2): 25–61

Allum JH, Mauritz KH (1984) Compensation for intrinsic muscle stiffness by short-latency reflexes in human triceps surae muscles. J Neurophysiol 52(5):797–818

Alvarez-Icaza R, Boahen K (2011) Deep cerebellar neurons mirror the spinal cord's gain to implement an inverse controller. Biol Cybern 105(1):29–40 doi:10.1007/s00422-011-0448-4

Amende I, Kale A, McCue S, Glazier S, Morgan JP, Hampton TG (2005) Gait dynamics in mouse models of Parkinson's disease and Huntington's disease. J Neuroeng Rehabil 2:20 doi:10.1186/1743-0003-2-20

Apps R, Garwicz M (2005) Anatomical and physiological foundations of cerebellar information processing. Nat Rev Neurosci 6(4):297–311 doi:10.1038/nrn1646

Aruin AS, Zatsiorsky VM (1984) Biomechanical characteristics of human ankle-joint muscles. Eur J Appl Physiol Occup Physiol 52(4):400–406

Becker JD, Mote CD Jr. (1990) Identification of a frequency response model of joint rotation. J Biomech Eng 112(1):1–8

Bennett DJ (1994) Stretch reflex responses in the human elbow joint during a voluntary movement. J Physiol 474(2):339–351

Bennett DJ, Hollerbach JM, Xu Y, Hunter IW (1992) Time-varying stiffness of human elbow joint during cyclic voluntary movement. Exp Brain Res 88(2):433–442

Berthier NE, Singh SP, Barto AG, Houk JC (1993) Distributed representation of limb motor programs in arrays of adjustable pattern generators. J Cogn Neurosci 5(1):56–78 doi:10.1162/jocn.1993.5.1.56

Blickhan, Full (1993) Similarity in multilegged locomotion: bouncing like a monopode. J Comp Physiol A 173(5):509–517

Bobet J, Stein RB (1998) A simple model of force generation by skeletal muscle during dynamic isometric contractions. IEEE Trans Biomed Eng 45(8):1010–1016 doi:10.1109/10.704869

Chorev E, Manor Y, Yarom Y (2006) Density is destiny—on [corrected] the relation between quantity of T-type Ca2+ channels and neuronal electrical behavior. CNS Neurol Disord Drug Targets 5(6):655–662

De Schutter E, Steuber V (2009) Patterns and pauses in Purkinje cell simple spike trains: experiments, modeling and theory. Neuroscience 162(3):816–826 doi:10.1016/j.neuroscience.2009.02.040

Devor A, Yarom Y (2002) Generation and propagation of subthreshold waves in a network of inferior olivary neurons. J Neurophysiol 87(6):3059–3069

Eyre JA, Miller S, Ramesh V (1991) Constancy of central conduction delays during development in man: investigation of motor and somatosensory pathways. J Physiol 434:441–452

Fujita M (1982) Adaptive filter model of the cerebellum. Biol Cybern 45(3):195–206

Ghez C, Fahn S (1985) The cerebellum. In: Kandel E, Schwarts J, Jessel T (eds) Principles of neural science, 2nd edn. Elsevier, New York

Gilbert PF, Thach WT (1977) Purkinje cell activity during motor learning. Brain Res 128(2):309–328

Gottlieb GL, Agarwal GC (1978) Dependence of human ankle compliance on joint angle. J Biomech 11(4):177–181

Herbin M, Gasc JP, Renous S (2004) Symmetrical and asymmetrical gaits in the mouse: patterns to increase velocity. J Comp Physiol A 190(11):895–906 doi:10.1007/s00359-004-0545-0

Hoffer JA, Andreassen S (1981) Regulation of soleus muscle stiffness in premammillary cats: intrinsic and reflex components. J Neurophysiol 45(2):267–285

Hunter IW, Kearney RE (1982) Dynamics of human ankle stiffness: variation with mean ankle torque. J Biomech 15(10):747–752

Ito M, Kano M (1982) Long-lasting depression of parallel fiber-Purkinje cell transmission induced by conjunctive stimulation of parallel fibers and climbing fibers in the cerebellar cortex. Neurosci Lett 33(3):253–258

Izhikevich EM (2007) Dynamical systems in neuroscience: the geometry of excitability and bursting (Computational Neuroscience). MIT Press, Cambridge

Jacobson GA, Lev I, Yarom Y, Cohen D (2009) Invariant phase structure of olivo-cerebellar oscillations and its putative role in temporal pattern generation. Proc Natl Acad Sci USA 106(9):3579–3584 doi:10.1073/pnas.0806661106

Kawato M, Gomi H (1992) A computational model of four regions of the cerebellum based on feedback-error learning. Biol Cybern 68(2):95–103

Kitazawa S, Kimura T, Yin PB (1998) Cerebellar complex spikes encode both destinations and errors in arm movements. Nature 392(6675):494–497 doi:10.1038/33141

Lacquaniti F, Licata F, Soechting JF (1982) The mechanical behavior of the human forearm in response to transient perturbations. Biol Cybern 44(1):35–46

Leznik E, Makarenko V, Llinas R (2002) Electrotonically mediated oscillatory patterns in neuronal ensembles: an in vitro voltage-dependent dye-imaging study in the inferior olive. J Neurosci 22(7):2804–2815

Llinas R, Walton K, Lang E (2004) Cerebellum. In: Sheperd G (ed) The synaptic organization of the brain. Oxford University Press, New York

Llinas R, Welsh JP (1993) On the cerebellum and motor learning. Curr Opin Neurobiol 3(6):958–965

Llinas R, Yarom Y (1986) Oscillatory properties of guinea-pig inferior olivary neurones and their pharmacological modulation: an in vitro study. J Physiol 376:163–182

Llinas RR (2009) Inferior olive oscillation as the temporal basis for motricity and oscillatory reset as the basis for motor error correction. Neuroscience 162(3):797–804 doi:10.1016/j.neuroscience.2009.04.045

Mano N, Kanazawa I, Yamamoto K (1986) Complex-spike activity of cerebellar Purkinje cells related to wrist tracking movement in monkey. J Neurophysiol 56(1):137–158

Manor Y, Rinzel J, Segev I, Yarom Y (1997) Low-amplitude oscillations in the inferior olive: a model based on electrical coupling of neurons with heterogeneous channel densities. J Neurophysiol 77(5):2736–2752

Marr D (1969) A theory of cerebellar cortex. J Physiol 202(2): 437–470

Mathy A, Ho SS, Davie JT, Duguid IC, Clark BA, Hausser M (2009) Encoding of oscillations by axonal bursts in inferior olive neurons. Neuron 62(3):388–399 doi:10.1016/j.neuron.2009.03.023

Ojakangas CL, Ebner TJ (1992) Purkinje cell complex and simple spike changes during a voluntary arm movement learning task in the monkey. J Neurophysiol 68(6):2222–2236

Schweighofer N, Doya K, Kawato M (1999) Electrophysiological properties of inferior olive neurons: a compartmental model. J Neurophysiol 82(2):804–817

Simpson JI, Wylie DR, De Zeeuw CI (1996) On climbing fiber signals and their consequence(s). Behav Brain Sci 19(3):384–389

Sinkjaer T, Hayashi R (1989) Regulation of wrist stiffness by the stretch reflex. J Biomech 22(11–12):1133–1140

Sinkjaer T, Toft E, Andreassen S, Hornemann BC (1988) Muscle stiffness in human ankle dorsiflexors: intrinsic and reflex components. J Neurophysiol 60(3):1110–1121

Weiss PL, Hunter IW, Kearney RE (1988) Human ankle joint stiffness over the full range of muscle activation levels. J Biomech 21(7):539–544

Welsh JP, Lang EJ, Suglhara I, Llinas R (1995) Dynamic organization of motor control within the olivocerebellar system. Nature 374(6521):453–457 doi:10.1038/374453a0

Welsh JP, Llinas R (1997) Some organizing principles for the control of movement based on olivocerebellar physiology. Prog Brain Res 114:449–461

Wetmore DZ, Mukamel EA, Schnitzer MJ (2008) Lock-and-key mechanisms of cerebellar memory recall based on rebound currents. J Neurophysiol 100 (4):2328–2347. doi:10.1152/jn.00344.2007

Widrow B, Walach E (1996) Adaptive inverse control. Prentice Hall information and system sciences series. Prentice Hall, Upper Saddle River, NJ

Yarom Y, Cohen D (2002) The olivocerebellar system as a generator of temporal patterns. Ann N Y Acad Sci 978:122–134

Zhang LQ, Nuber G, Butler J, Bowen M, Rymer WZ (1998) In vivo human knee joint dynamic properties as functions of muscle contraction and joint position. J Biomech 31(1):71–76